Molecular Cancer Therapeutics

ODM-203, a Selective Inhibitor of FGFR and VEGFR, Shows Strong Antitumor Activity, and Induces Antitumor Immunity

Tim H. Holmström[1], Anu-Maarit Moilanen[1], Tarja Ikonen[1], Mari L. Björkman[1], Tero Linnanen[1], Gerd Wohlfahrt[1], Stefan Karlsson[1], Riikka Oksala[1], Timo Korjamo[1], Susanta Samajdar[2], Srinivasan Rajagopalan[2], Shekar Chelur[2], Kishore Narayanan[2], Raghuveer K. Ramachandra[2], Jiju Mani[2], Rashmi Nair[2], Nagaraj Gowda[2], Thomas Anthony[2], Samiulla Dhodheri[2], Subhendu Mukherjee[2], Ravi K. Ujjinamatada[2], Nanduri Srinivas[2], Murali Ramachandra[2], and Pekka J. Kallio[1]

Abstract

Alterations in the gene encoding for the FGFR and upregulation of the VEGFR are found often in cancer, which correlate with disease progression and unfavorable survival. In addition, FGFR and VEGFR signaling synergistically promote tumor angiogenesis, and activation of FGFR signaling has been described as functional compensatory angiogenic signal following development of resistance to VEGFR inhibition. Several selective small-molecule FGFR kinase inhibitors are currently in clinical development. ODM-203 is a novel, selective, and equipotent inhibitor of the FGFR and VEGFR families. In this report we show that ODM-203 inhibits FGFR and VEGFR family kinases selectively and with equal potency in the low nanomolar range (IC_{50} 6–35 nmol/L) in biochemical assays. In cellular assays, ODM-203 inhibits VEGFR-induced tube formation (IC_{50} 33 nmol/L) with similar potency as it inhibits proliferation in FGFR-dependent cell lines (IC_{50} 50–150 nmol/L). *In vivo*, ODM-203 shows strong antitumor activity in both FGFR-dependent xenograft models and in an angiogenic xenograft model at similar well-tolerated doses. In addition, ODM-203 inhibits metastatic tumor growth in a highly angiogenesis-dependent kidney capsule syngenic model. Interestingly, potent antitumor activity in the subcutaneous syngenic model correlated well with immune modulation in the tumor microenvironment as indicated by marked decrease in the expression of immune check points PD-1 and PD-L1 on CD8 T cells and NK cells, and increased activation of CD8 T cells. In summary, ODM-203 shows equipotent activity for both FGFR and VEGFR kinase families and antitumor activity in both FGFR and angigogenesis models.

Introduction

The FGFR family consists of four highly conserved receptor tyrosine kinases (FGFR 1–4; refs. 1, 2). These regulate a wide range of physiologic processes, including embryonic development, tissue repair, angiogenesis, bone development, and regulation of phosphate homeostasis. The binding of FGF to FGFR leads to receptor dimerization and subsequent activation of downstream signaling pathways. Activated FGFR stimulates tyrosine phosphorylation and direct activation of a number of signaling molecules, including FGFR substrate 2 (FRS2; refs. 3, 4). This is followed by phosphorylation and activation of the Grb2/Sos1 complex and subsequent activation of the MAPK pathway (4, 5).

The oncogenic activity of FGFRs was originally described in connection with their capacity to directly promote endothelial cell proliferation and tumor angiogenesis (6, 7). In addition, several FGFR signaling components, such as FGF ligands, have been shown to be oncogenic in nonclinical models (2), and genetic alterations of FGFs and FGFRs have been identified in multiple tumor types (2, 8).

Angiogenesis is necessary for tumor growth, tissue invasion, and metastasis growth. VEGFs and FGF2 were among the first identified pro-angiogenic factors to have a direct promoting effect on tumor angiogenesis (6, 7). In animal studies, FGFR and VEGFR have been shown to act synergistically, resulting in fast-growing tumors (9). FGFR signaling also indirectly activates the VEGFR pathway, and activation of FGFR signaling functions as a compensatory angiogenic signal following development of resistance to VEGF inhibition (10–12).

Genetic alterations in FGFR and upregulation of VEGFR are often found in the same types of cancer—such as gastric, lung, and breast cancers—and the presence of these molecular alterations correlate with disease progression and unfavorable survival (12–24). This suggests a potential therapeutic advantage for

[1]Orion Corporation Orion Pharma, Finland. [2]Aurigene Discovery Technologies Limited, India.

Note: Supplementary data for this article are available at Molecular Cancer Therapeutics Online (http://mct.aacrjournals.org/).

Current address for T. Linnanen: Forendo Pharma, Turku, Finland; current address for R.K. Ujjinamatada: Organix Inc., Boston, Maine; and current address for N. Srinivas: National Institute of Pharmaceutical Education and Research (NIPER), Hyderabad, India.

Corresponding Author: Tim H. Holmström, Orion Corporation, Tengströminkatu 8, Turku 20101, Finland. Phone: 358104262838; E-mail: tim.holmstrom@orionpharma.com

doi: 10.1158/1535-7163.MCT-18-0204

selective dual inhibition of both FGFRs and VEGFRs in tumors with genomic aberrations in the FGFR signaling components.

Immune checkpoint inhibitors (anti-CTLA4, anti-PD1, and anti-PD-L1 antibodies), known to act by blocking the pathways that inhibit immune cell activation and thereby stimulating immune responses against the tumor cells, have been immensely successful in the treatment of several types of cancer. The abnormal tumor vasculature, induced by production of pro-angiogenic factors, supports an immunosuppressive tumor microenvironment enhancing the tumor potential to evade the host immunosurveillance (25, 26). Some proangiogenic factors such as VEGFR and FGFR may suppress the function of immune cells, and anti-angiogenic treatment may normalize the structure of intratumoral blood vessels enhancing the leukocyte-endothelial interaction, increasing the number of tumor-infiltrating lymphocytes (TIL) and reducing the number of myeloid-derived suppressor cells within the tumor (27–29). It is therefore possible that blocking the VEGFR and FGFR signaling pathway has an important effect on the tumor immune microenvironment.

Several compounds targeting FGFR have recently been evaluated in clinical trials. These have either been selective FGFR inhibitors or FGFR inhibitors with promiscuous kinase activity (8). In general, selective FGFR inhibitors have no effect on angiogenesis (8, 30–32), whereas the pankinase inhibitors have predominant activity toward the VEGFR family of kinases, thus masking their activity towards FGFR (33–36). Hence, there are theoretical and clinical reasons supporting the development of a selective FGFR and VEGFR inhibitor capable of suppressing both FGFR and VEGFR for the treatment of angiogenic tumors harboring genomic alterations in the FGFR pathway. In this study, we describe the preclinical pharmacology of ODM-203, a dual inhibitor of FGFR and VEGFR family of kinases that shows encouraging preliminary antitumor activity in the ongoing clinical trials in patients with advanced cancers (37).

Materials and Methods

All the animal experiments have been conducted in accordance with and approved by an Institutional Animal Care and Use Committee (IACUC).

All cell lines were obtained from ATCC and tested for mycoplasma using Venor GeM Mycoplasma Detection Kit (Sigma-Aldrich, MP0025). Cells were cultured according to the provider instructions. Typically cells were kept in culture for min. two passages prior and max. 20 passages when the experiments were performed. Cell line authentication was performed at Genomics Unit of Technology Centre, Institute for Molecular Medicine Finland (FIMM) with the Promega GenePrint10 System. All the cell lines had the same identity as the ATCC clones.

Compounds

ODM-203 was synthesized according to processes described in WO 2013 053983-Aurigene/Orion patent (Supplementary Fig. S1). AZD4547 was synthesized according to the processes described in the International Patent Application Publication Number WO2008/075068. Dovitinib (TKI-258) was synthesized according to processes described in the Patent, WO2006125130. Sorafenib has been purchased from Waterstone and Lucitanib from ChemScene.

In vitro kinase assays

The selectivity of the compounds was tested against 317 wild-type protein kinases at a concentration of 1 μmol/L with total 1 μmol/L ^{33}P-ATP (Perkin Elmer). Kinase inhibition IC_{50} values were determined for seven kinases with 10-dose IC_{50} mode starting at 1 μmol/L with a final concentration of 10 μmol/L ATP (Sigma) and ^{33}P-ATP mix. Specific kinase/substrate pairs along with the required cofactors were prepared in standard reaction buffer [20 mmol/L HEPES, pH 7.5, 10 mmol/L $MgCl_2$ (2 mmol/L $MnCl_2$ if applicable), 1 mmol/L EGTA, 0.02% Brij 35, 0.02 mg/mL BSA, 0.1 mmol/L Na_3VO_4, 2 mmol/L DTT, 1% DMSO]. After subtraction of background derived from control reactions containing inactive enzyme, kinase activity data were expressed as the percentage of remaining kinase activity in test samples compared with vehicle (dimethyl sulfoxide) reactions. IC_{50} values were obtained using Prism (GraphPad Software).

Cell viability assays

H1581 (ATCC-CRL-5878), Kato III (ATCC-HTB-103), SNU16 (ATCC-CRL-5974), and RT4 (HTB2) cell lines were obtained from ATCC and maintained in the cell culture media recommended by the supplier. For cell viability studies, cell lines were seeded at optimized cell density on assay plates in their respective growth media. The cells were allowed to attach overnight and then subsequently treated with the test compounds with an eight-dose concentration series up to 3 μmol/L for 96 hours. Cell proliferation was measured using the WST-1 Cell Proliferation Assay (Roche) and an Envision microplate reader (Perkin Elmer). Cell proliferation in the 0.5% DMSO control samples was considered to be the maximum and 300 nmol/L PD173074 (Sigma) was used as the full FGFR-inhibited proliferation control. The average of the 300 nmol/L PD173074 control values was subtracted from the individual sample values. Each concentration was studied in four replicates and inhibition of proliferation was expressed as a percentage of the DMSO control value. Normalized data were analyzed with XLFit4 software (IDBS) and a sigmoidal dose–response model was used to calculate the IC_{50} values. Average IC_{50} values were calculated from three independent experiments.

Cell-based angiogenesis assay

Angiogenesis inhibition with the test compounds was studied with VEGFR-driven tube formation in a GFP-AngioKit Cell Player kinetic coculture model of angiogenesis (Essen Biosciences). GFP-labeled human umbilical vein endothelial cells (HUVECs) were cocultured on two 96-well plates with human dermal fibroblasts for 2 days. Test compounds were added in the presence of 4 ng/mL VEGF to different wells using an eight-point concentration series from day 2. Vascular tube formation was monitored kinetically using an IncuCyte-FLR live-cell imaging system (Essen Biosciences). Fluorescent and phase-contrast images ($\times$10) were gathered every 12 hours for 10 days, and analyzed for tube length and number of branch points. Media and test agents were replaced every 2 to 3 days. Tube formation was analyzed using the IncuCyte angiogenesis algorithm. Data were further analyzed for IC_{50} values using Microsoft Excel (v7.0) by fitting the concentration response data to a four-parameter logistic fit.

Phospho-FRS2 Tyrosine 196 Assay

Inhibition of FRS2 Tyrosine 196 phosphorylation by ODM-203 in FGFR-dependent cell lines was measured using

an MSD 96-well multiarray Phospho-FRS2 Tyr196 assay (MesoScale Diagnostics) according to the manufacturer's instructions. Briefly, the cell lines were seeded at a density of 75,000 cells/well on poly-D-lysine-coated 96-well plates (Catalog no. 354461; Becton Dickinson) in the cell culture media recommended by the supplier. The cells were allowed to attach overnight and subsequently treated with the vehicle (0.5% DMSO) or increasing concentrations of ODM-203 for 20 minutes. The cell culture media were aspirated and the cells lysed in MSD Tris Lysis Buffer (Catalog no. R60TX-2; MesoScale Diagnostics) supplemented with 10 mmol/L NaF, 1× phosphatase inhibitor cocktail 2 and 3 (Catalog nos. P5726 and P0044; Sigma) and Complete Protease Inhibitor Cocktail (Catalog no. 1836170; Roche). The electrochemiluminescence signal was detected with a SECTOR Imager 2400 plate reader (MesoScale Diagnostics) coupled to a CCD camera. Data were expressed as percentages of vehicle control values and analyzed with GrapPadPrism 7.03 (GraphPad Software). Each test concentration was studied at least in triplicate and inhibition percentages were calculated for the parallel samples. Average IC_{50} values were calculated from two independent experiments.

Immunoblotting

HUVEC cells (Life Sciences) were serum-starved with 1% FBS overnight, treated for 1 hour with ODM-203, and then 20 ng/mL VEGF (Sigma) was added for 10 minutes. The SNU16 cell line (ATCC) was treated for 1 hour with ODM-203. HUVEC samples were immunoblotted with phosphorylated VEGFR2 (Cell Signaling Technology) and VEGFR2 (R&D Systems). SNU16 samples were immunoblotted with phosphorylated FGFR (Cell Signaling Technology) and FGFR2 (Abcam) antibodies.

Subcutaneous xenograft models

Athymic Nude-Foxn1nu female mice (9 weeks old; Harlan, the Netherlands) were subcutaneously injected with 1 million H1581, KMS11, RT4, or SNU16 cells in 100 μL of McCoy's 5a modified medium and Matrigel (BD) (1:1). Tumor growth was monitored twice weekly by caliper measurements. Oral treatment with ODM-203 and AZD-4547 was started when the average tumor volume reached 100 mm^3 and continued for 21 days for the RT4 xenograft model ($n = 12$/group) and 12 days for the SNU16 xenograft model ($n = 6$/group). Necropsy, and plasma and tumor sampling were carried out 4 hours after the last dosing.

Doses for 12.5 mg/kg AZD4547 and 40 mg/kg sorafenib were chosen based on published data [26, 32]. Oral treatment (ODM-203 or AZD4547) was initiated when the average tumor volume reached ≈125 mm^3. Mean tumor volumes were calculated for each treatment group.

Orthotopic Renca syngenic model

0.15 million Renca (mouse renal carcinoma; CRL-2947) cells in 40 μL of RPMI1640 media and Matrigel (1:1) were injected into the subcapsular area of the left kidney of balb/c male mice (8 weeks old; Aurigene). Treatments were started 2 days after surgery ($n = 10$ per group). Animals were sacrificed after 21 consecutive days of daily oral dosing with ODM-203, Sorafenib, or AZD-4547. There were 10 animals in each group. Mean tumor weight was measured after 21 days for each treatment group. Lung nodules were counted at necropsy.

Staining for CD31 in the syngenic Renca model

Five-micrometer paraffin-embedded sections of tumor tissues were used for analysis. Sections were deparaffinized followed by antigen retrieval in citrate buffer pH 6.0 for 30 minutes (Target retrieval solution; DAKO). These sections were then subjected to endogenous peroxidase block (1% H_2O_2) for 30 minutes followed by blocking with 10% goat-serum for 1 hour at room temperature. This was followed by avidin–biotin block for 15 minutes each. After the washing and blocking steps, tumor sections were incubated overnight at 4 °C with anti-mouse CD31 antibody (1:300 dilution; Abcam AB28364), followed by incubation with biotinylated anti-rabbit secondary antibody (1:500 dilution) at room temperature for 1 hour. Immunoreactivity was visualized with the Vectastain ABC System and 3,3-diaminobenzidine (Vector Laboratories). The slides were finally washed for 5 minutes in water and then counterstained with hematoxylin. Then slides were then dehydrated, mounted using DPX mount, and viewed under a light microscope. All sections were photographed with a digital camera.

Immune pharmacodynamic analysis in subcutaneous Renca syngenic model

For the measurement of immune pharmacodynamics (PD), Renca cell lines were subcutaneously implanted into 5 to 7 weeks old male Balb/c mice by injecting 1 million Renca tumor cells/animal. When tumor volume reached ∼182 to 190 mm^3, animals were randomized and allocated to four treatment groups ($n = 5$). Mice were orally treated daily with vehicle and ODM-203 (20 and 40 mg/kg) for 5 days. As an additional control, anti-PD1 antibody (100 μg/animal, clone J43) was dosed intraperitoneally on day 1. After 24 hours of last dosing, animals were sacrificed and blood samples and tumor tissues were collected from each animal and processed for PD evaluation.

Around 100 μL of blood from each animal was added in a round-bottom 96-well plate and RBC lysis was performed by adding 100 μL of ACK lysis buffer (NH_4Cl 8,024 mg/L; $KHCO_3$ 1,001 mg/L; EDTA $Na_2{\cdot}2H_2O$ 3.722 mg/L, pH 7.2) and incubating at 37 °C for 5 minutes. Plate was centrifuged at 300 × *g* for 5 minutes. Cells were washed two times using 1× PBS, pH 7.2 and used for antibody staining.

Tumor tissues were minced using sterile scissors/blades and forceps and were treated with 2 to 2.5 mL of tumor dissociation buffer (Miltenyi Biotech) and incubated for 30 minutes at 37 °C. After incubation, cell preparation was washed once with 1× PBS by centrifuging at 200 × *g* for 10 minutes. Cell pellet was suspended in 1× PBS and filtered through 70-μm cell strainer to remove debris. Cells were washed with 1× PBS and layered onto Histopaque (Sigma) and centrifuged at 400 × *g* for 20 minutes for isolating TILs. TILs layer was carefully collected and washed twice with 1× PBS.

Cells from blood and TILs were stained with the following antibodies from eBioscience: FITC-conjugated anti-mouse CD4, PE-conjugated anti-mouse CD25, PE-Cy7-conjugated anti-mouse CD3, APC-conjugated anti-mouse FoxP3, FITC-conjugated anti-mouse CD49b, PE-conjugated anti-mouse CD45, PE-conjugated anti-mouse IL2, and APC-conjugated anti-mouse IFNγ from Biolegend: APC-Cy7-conjugated anti-mouse CD8, BV-510-conjugated CD45, and BV-421-conjugated anti-mouse CD274.

Staining of cell surface markers was done by using respective antibodies prepared in FACS staining buffer (eBioscience) and added to respective panel tubes and incubated for 30 minutes at

4°C under dark. After incubation, cells were washed using FACS staining buffer and resuspended in FACS staining buffer and acquired using FACSVerse flow cytometer (BD Biosciences). Intracellular staining for regulatory T cells and cytokines was done by following manufacturer's protocol with modifications. Briefly, cells were stained first for cell surface markers using respective antibodies by following above protocol. Surface stained cells were fixed using 1× fixation/permeabilization buffer followed by permeabilization using 1× permeabilization buffer and stained for intracellular marker (FoxP3) or for cytokines (IL-2 and IFN-γ) by incubating samples with respective antibodies for 30 min at 4 °C. For cytokine analysis cells from blood and TILs were stimulated *ex vivo* with PMA (50 ng/mL) and ionomycin (500 ng/mL) for 6 hours in the presence of brefaldin-A. After staining, cells were washed twice with permeabilization buffer and finally resuspended in FACS staining buffer and acquired using flow cytometer. Appropriate compensation controls, isotype controls or fluorescence minus one (FMO) controls and unstained samples were used for FACS analysis. FACS analysis was performed with FACSuite software (v1.0.5.3841; BD Biosciences) by gating on appropriate population using respective controls. Outliers from each treatment group were determined by Grubb's method. Outliers were excluded and data from treatment groups were compared to vehicle-treated group and one-way ANOVA with Dunnett's multiple comparisons test was performed for statistical significance. All statistical analyses were performed using GraphPad Prism 7 and $P < 0.05$ was considered as statistically significant. Statistically significant differences, were designated by the asterisks as stated: *, $P < 0.05$; **, $P < 0.01$; ***, $P < 0.001$; ****, $P < 0.0001$.

In vitro assessment of PD-L1 expression on Renca cells with ODM-203 treatment was performed by flow cytometry. Briefly, 50,000 Renca cells/well were seeded on day 0 in a six-well plate. Next day, adherent cells were washed once with culture media and treated with indicated concentrations of ODM-203 for 1 hour at 37 °C. After incubation, media was replaced with fresh culture media without compound and further incubated for 16 hours.

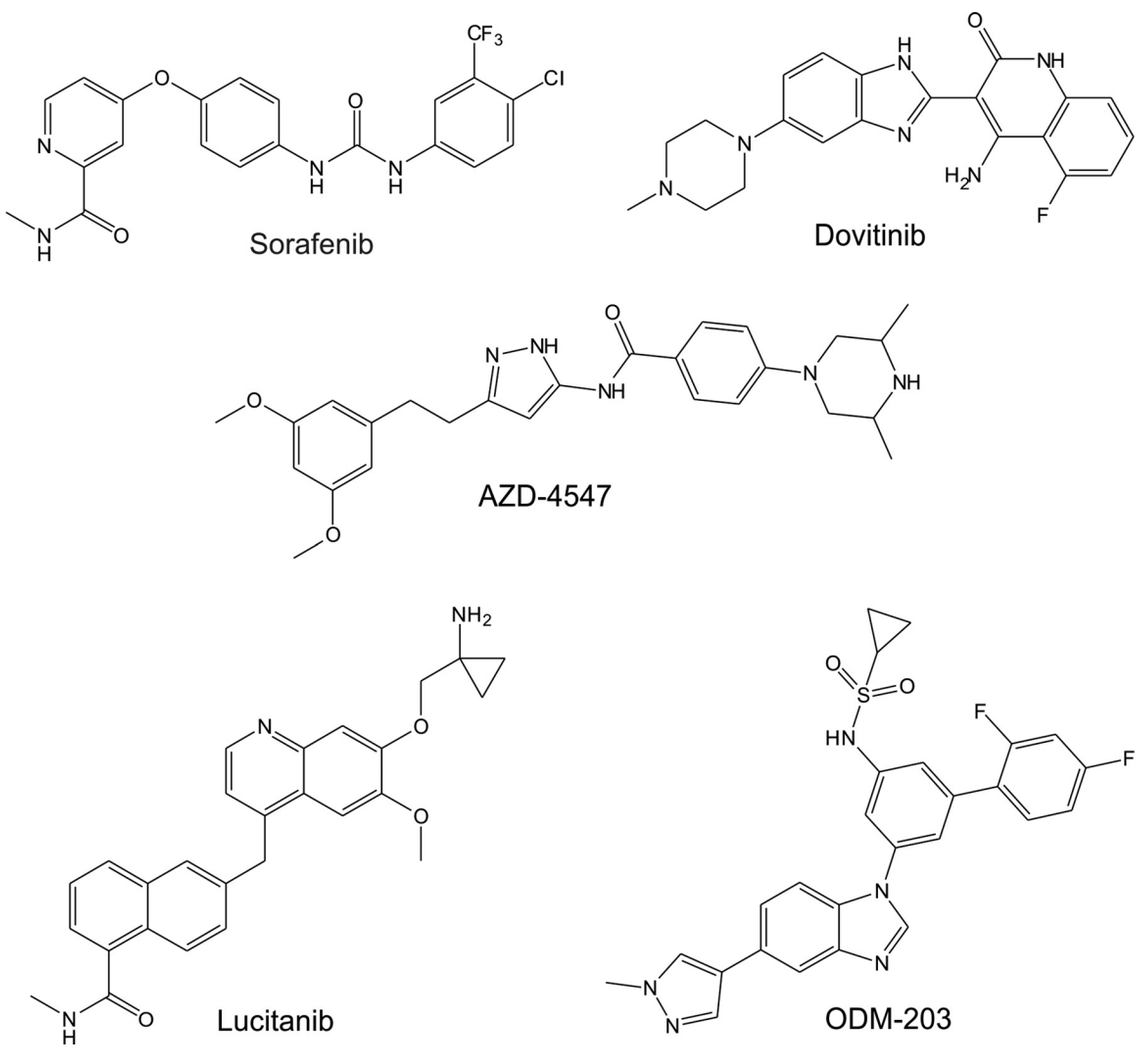

Figure 1.
Chemical structures of ODM-203 and the reference compounds described in this article.

Cells were harvested and stained with anti-PD-L1 antibody, staining protocol was followed as above and acquired using FACSVerse flow cytometer (BD Biosciences).

Results

ODM-203 is a potent and selective inhibitor of FGFR and VEGFR tyrosine kinases

The activity of ODM-203 (Fig. 1) towards its primary targets was measured using standard radiometric kinase assays with recombinant proteins. In these studies, ODM-203 showed approximately equal potency towards recombinant FGFR1, 2, 3, and 4, as well as VEGFR1, 2, and 3, with IC_{50} values in the low nanomolar range (Table 1A). Lucitanib (Fig. 1) was less potent (×5) towards FGFR1 than VEGFR2 (Table 1A), which is in line with previously published data [31]. Broad *in vitro* kinase selectivity of ODM-203 was examined towards 317 human kinases at a concentration of 1 μmol/L. In addition to its primary targets, ODM-203 suppressed 9/317 additional kinases by >70%, whereas the FGFR inhibitors AZD-4547 and dovitinib (Fig. 1; Supplementary Table S1) suppressed 39 and 74 kinases respectively in the same assay. Six of the nine kinases suppressed by ODM-203—DDR1, MAP4K4, MINK1, RET, PDGFRa, and SIK2—were suppressed at IC_{50} <100 nmol/L (Table 1B).

ODM-203 is a potent inhibitor of FGFR signaling and proliferation in several FGFR-dependent cell lines

Next, we studied the potency and selectivity of ODM-203 in cellular assays. The ability of ODM-203 to inhibit growth of FGFR-dependent cancer cells was studied by measuring inhibition of cell proliferation in three different well-characterized FGFR-dependent cell lines, each having genomic alteration in one of the FGFR subtypes 1 to 3, leading to overexpression of the respective FGFR. The H1581 cell line originates from a primary large-cell lung cancer specimen. It has an amplification on chromosome 8p12, which leads to multiple copies and, thus, to overexpression of the FGFR1 gene (38). The SNU16 gastric cancer cell line contains an FGFR2 gene amplification which leads to overexpression and constitutive activation of the receptor (39). The RT4 cell line is a bladder cancer cell line in which chromosomal rearrangement results in FGFR3–TACC3 fusion transcripts that make the cell line highly dependent on FGFR3 (40). ODM-203 suppressed cell proliferation in a dose-dependent manner in H1581, SNU16, and RT4 cells. IC_{50} values ranged from 104 nmol/L in H1581 cells to 192 nmol/L in RT4 cells (Table 2A). Similar results were obtained with lucitanib (Table 2A). Notably, proliferation of cell lines having no identified defects in FGFR expression or signaling were unaffected by incubation with ODM-203 up to a concentration of 3 μmol/L (Table 2B). These studies indicated that ODM-203 can efficiently inhibit proliferation of FGFR-dependent cell lines.

ODM-203 is equally potent in inhibiting VEGF-induced cellular tube formation and FGFR-dependent cell proliferation

VEGFRs regulate angiogenesis both during development and under pathologic conditions such as tumor formation (41–43). Therefore, the initial VEGFR kinase activity of ODM-203 was further verified by its ability to inhibit angiogenesis in the VEGF-induced tube formation assay (44, 45). ODM-203 inhibited endothelial tubule formation in a dose-dependent manner at nontoxic concentrations with an IC_{50} value of 33 nmol/L. In our hands, lucitanib, with an IC_{50} of 1 nmol/L, was more potent in suppressing VEGFR-induced tube formation than ODM-203 (Table 2A). Taken together, ODM-203 showed similar potency in inhibiting both VEGFR-driven cellular tube formation and suppressing FGFR-dependent cell proliferation, reflected in an IC_{50} ratio of 1:4, whereas lucitanib (IC_{50} ratio approximately 1:120) was clearly less potent at suppressing FGFR-dependent cell proliferation than VEGFR-induced cellular tube formation.

Capability of ODM-203 to inhibit cell proliferation in FGFR-dependent cell lines correlates with inhibition of FGFR signaling

FGFR signaling depends on autophosphorylation of FGFR followed by Tyr-phosphorylation of the adapter protein FRS2, which in turn activates downstream effector kinases (46). To verify the mechanism by which ODM-203 exerts its antiproliferative activity *in vitro*, the ability of ODM-203 to inhibit FGFR signaling was studied by measuring tyrosine 196 (Tyr196) phosphorylation of FRS2 in the FGFR-dependent cancer cell lines H1581 (FGFR1), SNU16 (FGFR2), and RT4 (FGFR3). ODM-203 dose-dependently inhibited FRS2 Tyr196 phosphorylation with IC_{50} values 93 nmol/L (H1581), 59 nmol/L (SNU16), and 89 nmol/L (RT4; Supplementary Fig. S2). This study shows that reduced proliferation of FGFR-dependent cell lines in response to ODM-203 is accompanied by inhibition of FGFR signaling, indicating that the effects of ODM-203 on proliferation of FGFR-responsive cell lines is likely to be caused by inhibition of FGFRs.

ODM-203 is equally potent at inhibiting FGFR and VEGFR cellular signaling

The intended target population of ODM-203 is cancer patients having an angiogenic tumor with a genetic alteration in the

Table 1. ODM-203 is selective and equally potent against recombinant FGFR and VEGFR family kinases

A			B	
IC_{50} (nmol/L)	ODM-203	Lucitanib	Kinase	IC_{50} (nmol/L)
FGFR1	11	58	DDR1	6
FGFR2	16	186	MAP4K4	49
FGFR3	6	253	MINK1	41
FGFR4	35	>1,000	RET	8
VEGFR1	26	162	PDGFRa	35
VEGFR2	9	9	PDGFRb	169
VEGFR3	5	34	SIK2	23
Ratio FGFR1/FGFR2	1:1	1:5	YES1	152
			TIE2	174

NOTE: (A) The IC_{50} values of ODM-203 and lucitanib for FGFR and VEGFR were determined using a standard radiometric assay. (B) IC_{50} values for the nine additional kinases of the 317 tested that ODM-203 inhibited by >70% at a concentration of 1 μmol/L. Each value is the mean of at least three independent experiments and three repetitions.

Table 2. ODM-203 is slightly more potent at inhibiting FGFR-dependent cell proliferation than VEGF-driven tube formation in a cellular assay

A

Proliferation IC_{50} nmol/L cell line (receptor)	ODM-203	Lucitanib
H1581 (FGFR1)	104	160
SNU16 (FGFR2)	132	65
RT4 (FGFR3)	192	130
Angiogenesis (VEGFR)	33	1
Ratio FGFR/Angiogenesis	1:4	1:120

B

Compound IC_{50}, nmol/L	A431	H1975	Miapaca-2	HCT116	Vcap	Renca
ODM-203	55% at 10 μmol/L. No inhibition at ower doses	45% at 10 μmol/L. No inhibition at lower doses	45% at 10 μmol/L. No inhibition at lower doses	37% at 10 μmol/L. No inhibition at lower doses	>3 μmol/L	22% at 10 μmol/L

NOTE: (A) Summary of in vitro antiproliferative IC_{50} values for ODM-203 and lucitanib obtained using a standard metabolism-based proliferation assay in three different FGFR1–3-dependent cell lines (H1581, SNU16, and RT4), as well as ODM-203, and lucitanib's capacity to inhibit VEGF-driven tube formation. (B) ODM-203 does not affect cell proliferation of control cell lines, having no identified defects in FGFR expression or signaling. Each value is the mean of at least three independent experiments and three repetitions.

FGF/FGFR signaling pathway. To mimic the above-described tumors in a cellular system, we compared the effect of ODM-203 at suppressing autophosphorylation of FGFR on Tyr653/654 in the FGFR2-dependent SNU16 cells (Fig. 2A) with the effect of ODM-203 at suppressing autophosphorylation of VEGFR on Tyr1054 phosphorylation in HUVEC cells treated with VEGF (Fig. 2B). The results confirm that ODM-203 suppresses both FGFR and VEGFR signaling at concentrations corresponding to its antiproliferative effect in FGFR-dependent cell lines and suppression of cellular tube formation. Importantly, these results also verify that ODM-203 shows similar potency towards FGFR and VEGFR kinases in cells.

ODM-203 inhibits FGFR phosphorylation and tumor growth in several FGFR-dependent xenografts

The *in vivo* efficacy of ODM-203 in FGFR-dependent models was evaluated in subcutaneous H1581, KMS11, RT4, and SNU16 xenografts (Fig. 3; Supplementary Fig. S3). Treatment with ODM-203 for 21 consecutive days significantly inhibited tumor growth when compared with the vehicle-dosed mice (Fig. 3A). The observed tumor growth inhibition (TGI) in RT4 xenografts was 37% and 92% with 20 and 40 mg/kg/day of ODM-203, respectively (Fig. 3B). The FGFR-dependency of this model was confirmed by the significant inhibition of tumor growth achieved with once-daily doses of the selective FGFR inhibitor AZD4547 (ref. 30; Fig. 3A). In the FGFR2-dependent xenograft model using SNU16 cells, 12 consecutive days of daily dosing with ODM-203 was associated with clear suppression of pFGFR and pFRS2 signals in the tumor which, correlating with statistically significant inhibition of tumor growth (Figs. 3B and C; Supplementary Fig. S4). The observed TGI was 73% (Fig. 3B). In addition, ODM-203 showed antitumor activity in the FGFR-dependent H1581 and KMS11 subcutaneous xenograft models (Supplementary Fig. S3) and inhibited pFGFR signaling 8 hours after dosing in the KMS11 xenograft model (Supplementary Fig. S5). Taken together, this suggests that ODM-203 activity in FGFR-dependent *in vivo* tumor models is attributable to its capability to suppress FGFR signaling in tumors.

ODM-203 shows strong antitumor activity in a VEGFR-dependent angiogenic orthotopic syngenic model (Renca)

In the angiogenesis-dependent syngeneic model (47), tumors were established by injection of mouse Renca cells orthotopically into the right kidney of BALB/c mice. Treatments were started when the animals had recovered from surgery for 2 days. Following 21 consecutive days of oral daily dosing with ODM-203 at doses of 7, 20, or 40 mg/kg, the observed TGI was 39%, 58%, and 75%, respectively (Fig. 4A). One daily dose of ODM-203 (40 mg/kg) significantly inhibited primary tumor growth ($P < 0.01$; Fig. 4A). The angiogenesis dependency of this model was confirmed as sorafenib, a classical VEGFR inhibitor (47), showed significant tumor inhibition whereas the selective FGFR inhibitor AZD4547 did not show any activity in this model (Fig. 4A). ODM-203 also inhibited formation of lung metastasis, as demonstrated by counting the number of lung nodules at necropsy (Fig. 4B). When staining the tumor sections at the end of the study for CD31, we observed a decrease in CD31 expression in the tumor treated with ODM-203 (Supplementary Fig. S6). This further indicates that ODM-203 suppresses angiogenesis at doses showing antitumor activity *in vivo*.

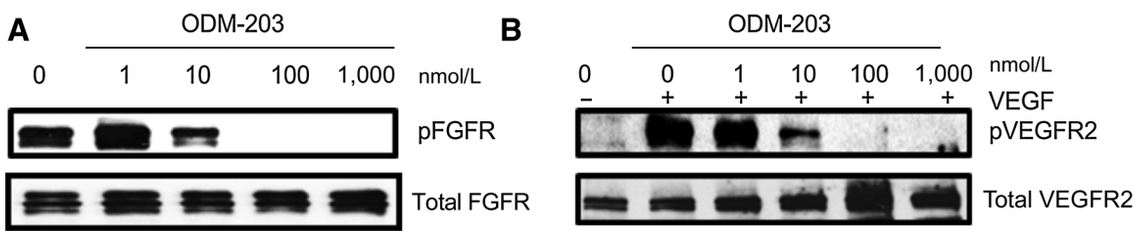

Figure 2.

ODM-203 is equally potent at inhibiting FGFR and VEGFR phosphorylation in cells. **A,** Effect of ODM-203 on FGFR phosphorylation in an FGFR-dependent cell line (SNU16). **B,** Effect of ODM-203 on VEGFR phosphorylation in HUVEC cells. Each value is the mean of at least three independent experiments and three repetitions.

ODM-203 activates immune response in the tumor microenvironment

In view of the potent antitumor activity in the syngenic kidney capsule Renca model and earlier reports indicating a role for inhibitors of tyrosine kinases including VEGFR (48) and FGFR (49), we sought to characterize the impact of ODM-203 on immune cells in circulation and tumor microenvironment in the Renca subcutaneous tumor model. Analysis of immune population in the blood indicated that ODM-203 treatment resulted in an increase in the percentage of total and CD4 T cells (Fig. 5A). Considering that regulatory T cells within the CD4 T cells could be immunosuppressive, we further analyzed the regulatory T cells (CD25 and FoxP3 double positive cells). Results revealing a significantly higher ratio of total T cells to regulatory T cells indicate that increased T cells are predominantly effector in nature (Fig. 5A). Analysis of TILs showed a decrease in the expression of immune check points PD-1 and PD-L1 and a concomitant increase in IFNγ expression on both CD8 T cells and NK cells (Fig. 5B) indicating immune activation within the tumor due to ODM-203 treatment. Furthermore, ODM-203 treatment of Renca cells *in vitro* reduced PD-L1 expression on these tumor cells (Supplementary Fig. S7).

Discussion

In this paper, we have reported the pharmacologic profile of ODM-203, a novel, selective FGFR and VEGFR family kinase inhibitor. Several kinase inhibitors with anti-FGFR activity have been described previously. These include selective FGFR inhibitors (8, 30–32) and pan-kinase VEGFR2 inhibitors that have either been approved or are in clinical development as anti-angiogenic agents (34–36). Some of the pan-kinase VEGFR2 inhibitors also show activity towards FGFR in nonclinical models (34–36). However, in clinical studies, pan-kinase VEGFR inhibitors show angiogenesis-related adverse events which hampers increasing the dose to a level at which FGFR activity would be suppressed.

There are several lines of evidence suggesting that dual inhibition of FGFR and VEGFR could be advantageous in defined tumors. First, several of the tumor types in which FGFR genomic alterations have been described are known to be angiogenic (12–24). Second, FGFR and VEGFR are known to crosstalk and act synergistically in nonclinical models and upregulation of FGFRs is a known escape mechanism from treatment with VEGFR inhibitors (9, 11, 12, 43). In these particular tumors, the simultaneous inhibition of VEGFR and FGFR could be advantageous.

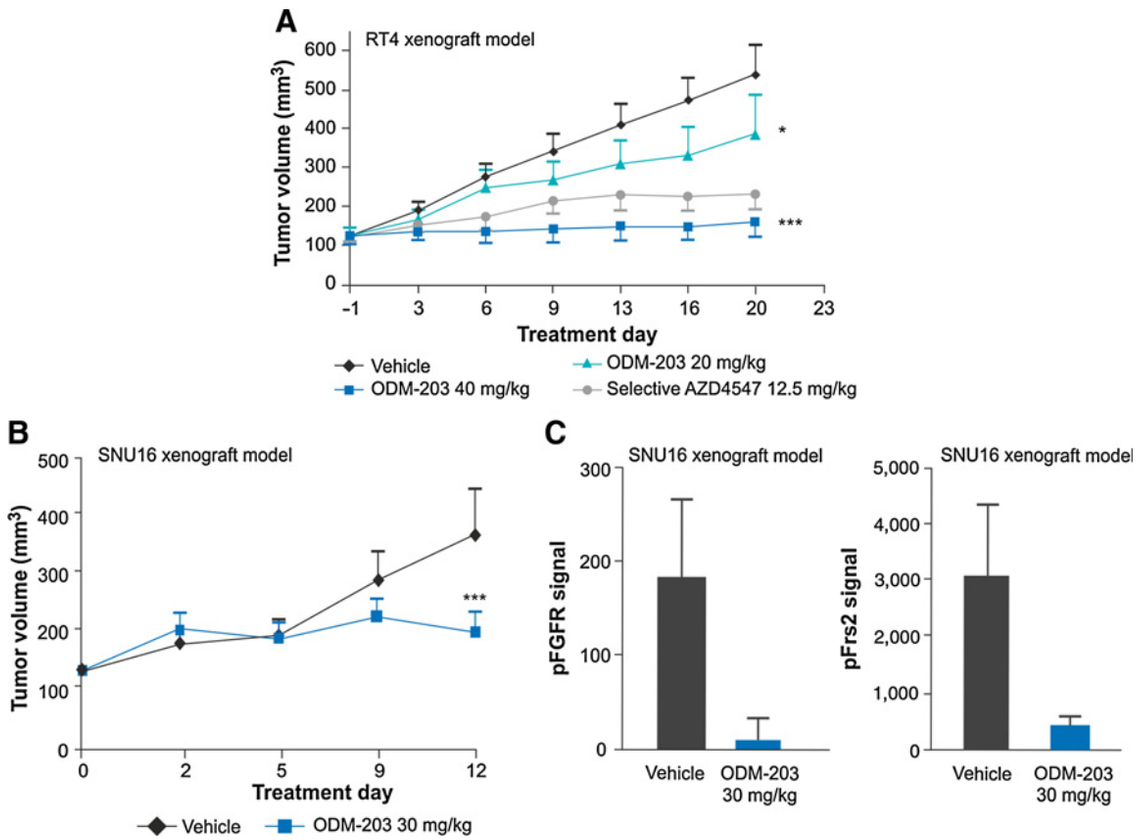

Figure 3.

ODM-203 suppresses *in vivo* tumor growth and FGFR signaling in FGFR-dependent tumor models. Effect of ODM-203 on the tumor volumes (**A**) of animals bearing subcutaneous RT4 tumors during 21 days of oral treatment with ODM-203 at doses of 20 and 40 mg/kg. Effect of ODM-203 on the tumor volume (**B**), phosphorylation of FGFR (**C**), and phosphorylation of FRS2-bearing subcutaneous SNU16 tumors (**C**) after 12 days of oral treatment with ODM-203 at a dose of 30 mg/kg. TGI (%) in both models is indicated in part (**A** and **B**). Tumor samples were fixed 4 hours after last dosing. $^{***}P < 0.001$ and $^{*}P < 0.05$ for differences between experimental groups and vehicle (control) as determined by analysis of variance with one factor (treatment). Average tumor volumes are plotted as bars, and error bars represent the SEM.

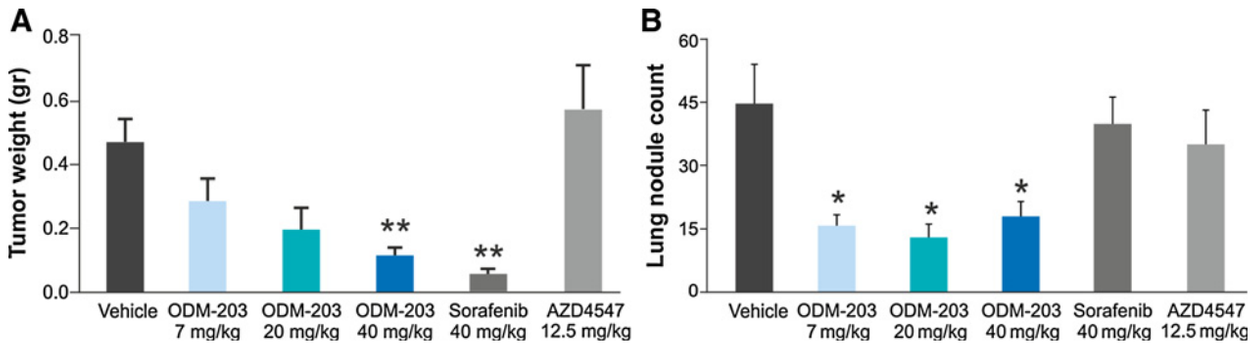

Figure 4.

ODM-203 has strong *in vivo* antitumor activity in an angiogenic model. Effect of ODM-203 on the tumor weights (**A**) and lung nodules (**B**) of animals bearing orthotopic Renca tumors after 21 days of oral treatment at doses of 7, 20, and 40 mg/kg. The observed primary TGI was 75% (**A**). $^{**}P < 0.01$ and $^{*}P < 0.05$ for differences between experimental groups and vehicle (control) as determined by analysis of variance with one factor (treatment). Average tumor volumes are plotted as bars, and error bars represent the SEM.

In this paper, we have described the pharmacologic profile of ODM-203, a novel, selective dual FGFR and VEGFR family kinase inhibitor. ODM-203 is unique as it is equally potent for both FGFR and VEGFR family kinases, and inhibits a limited number of additional kinases. The results of the *in vitro* kinase assays were corroborated in cellular studies: ODM-203 suppresses proliferation of several well-characterized FGFR-dependent cell lines, namely H1581, SNU16, and RT4, as well as VEGFR-induced tube formation at similar concentrations. The target-specific activity of ODM-203 was also demonstrated in cell-based studies in which it suppressed FGFR and VEGFR signaling at concentrations corresponding to its capability to suppress cell proliferation in FGFR-dependent cells and VEGFR-induced tube formation. ODM-203 also suppressed phosphorylation of the direct downstream target pFRS2 in H1581, SNU16, and RT4 cells at concentrations corresponding closely to the antiproliferative activity in the same cell line. Furthermore, ODM-203 inhibited autophosphorylation of FGFR in the FGFR2-dependent cell line SNU16 and VEGFR in HUVEC cells treated with VEGF at similar concentrations. Consistent with the above-mentioned studies, ODM-203 did not affect cell proliferation in cells that do not have identified defects in FGFR expression or signaling.

The *in vitro* selective inhibition of FGFR and VEGFR was further validated in a series of *in vivo* xenograft studies. The FGFR-dependent *in vivo* models used were the RT4 and SNU16 subcutaneous xenograft models (30–32). In the FGFR3-dependent RT4 model, treatment with ODM-203 led to a significant reduction in tumor growth in a dose-dependent manner and, in the SNU16 model, reduction in tumor growth was accompanied by suppression of FGFR signaling in the tumors. It is therefore likely that ODM-203 inhibits tumor growth in FGFR-dependent models by suppressing FGFR signaling *in vivo*. To further evaluate the *in vivo* activity of ODM-203 in angiogenic tumors, we used a well-characterized angiogenic orthotopic and syngeneic model: the Renca model (47). This model also has the advantage of being metastatic. As expected from our *in vitro* data, treatment with ODM-203 led to a significant reduction in tumor growth in a dose-dependent manner. In this model, we also found potent and significant inhibition of formation of lung metastases. Taken together, ODM-203 shows good, balanced potency towards both FGFR and VEGFR *in vitro*, which translates into similarly balanced *in vivo* potency in angiogenic and FGFR-dependent tumor models.

In view of the remarkable success with the immune-based therapeutic approaches, we also evaluated the impact of ODM-203 on immune cells in circulation and in the tumor in the syngenic subcutaneous Renca model. In addition to a significant elevation in the ratio of total T cells with respect to regulatory T cells in circulation, we also observed a dramatic reduction in the percentage of PD-1 and PD-L1 expressing CD8 T cells and NK cells favoring an antitumor immune response. Consistent with these changes, the total number of IFNγ positive CD8 T cells and NK cells in the tumor was also elevated. These results indicate that in a model such as Renca that is not dependent on FGFR, observed antitumor and antimetastastic activity are likely due to a combination of anti-angiogeneis and antitumor immune response effects. Immune activation observed in the tumor microenvironment upon ODM-203 is consistent with reported immune activation by inhibitors of tyrosine kinases including VEGFR (48) and FGFR (49). In this context, a direct comparison of inhibitors selectively targeting FGFR or VEGFR or dually targeting both these kinase families such as ODM-203 will be of interest for future studies, and may help in appropriate clinical positioning of ODM-203.

Tyrosine kinase inhibitors (TKI) mediate an antitumor immune response likely by two mechanisms; immunogenic modulation and by immune subset conditioning. Immunogenic modulation is characterized by an increase in tumor cell sensitivity to immune cell-mediated lysis through an alteration in tumor cell phenotype. In this context, Cabozantinib was shown to improve the sensitivity of murine and human tumor cells to T-cell–mediated lysis (50). Although immune subset conditioning, which applies to both the peripheral immune system and the tumor microenvironment, denotes an alteration in the frequency and/or function of immune cell subsets, thus supporting more productive immune interactions (51). TKIs such as Pazopanib and Sunitinib are reported to skew the immune response from a Th2 to antitumor Th1 response (52, 53). In a preclinical model, Cabozantinib treatment showed an increase in the number of $CD4^+$ and $CD8^+$ T cells

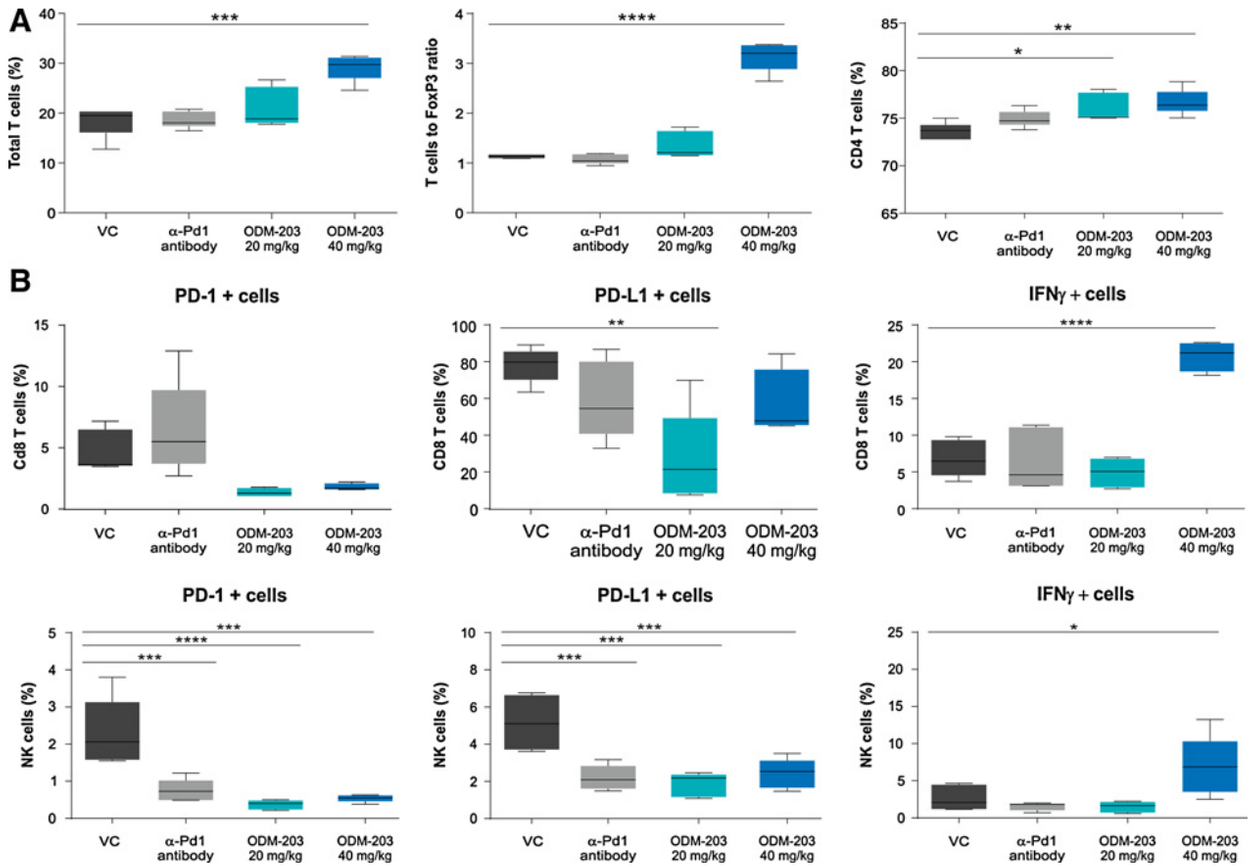

Figure 5.

ODM-203 administration results in immune activation in a syngenic model. Effect of ODM-203 on T cells in circulation (**A**) and TILs (**B**) in the Renca subcutaneous tumor model after 5 days of oral treatment at doses of 20 and 40 mg/kg is presented as a box and whisker plot. Each box indicates the numerical data through their quartiles for each group, and the whiskers (lines extending vertical from the boxes) are used to indicate variability outside the upper and lower quartiles. Different immune cells in blood were analyzed by gating FSC-SSC plot followed by doublets exclusion. Resultant singlets were further gated on $CD3^+$ (total T cells) and then on $CD4^+$ (CD4 T cells). FoxP3 regulatory T cells were analyzed by gating CD25 and FoxP3 double positive cells in CD4 T cells. TILs were analyzed by gating FSC-SSC plot followed by singlets gate. Within singlets, cells were further gated on $CD45^+$ and then on $CD3^+$ (total T cells) and $CD49b^+$ (NK cells). Total T cells were further gated on $CD8^+$ to determine CD8 T cells. CD8 T cells expressing PD-1 and PD-L1 were analyzed by gating on $CD8^+PD\text{-}1^+$ and $CD8^+PD\text{-}L1^+$ double positive cells within CD3 gate. Similarly, for NK cells, $CD49b^+PD\text{-}1^+$ and $CD49b^+PD\text{-}L1^+$ double positive cells were gated on CD45 population. Percent PD-1 positive and PD-L1 positive CD8 T cells and NK cells are plotted. For IFNγ-secreting CD8 T cells and NK cells, gates were directly applied from $CD8^+$ and $CD49b^+$, respectively. *, $P < 0.05$, **, $P < 0.01$, ***, $P < 0.001$, ****, $P < 0.0001$. VC, vehicle control.

with a concomitant decrease in the percentage of splenic T-regulatory cells (Tregs) and myeloid-derived suppressor cells (MDSC; ref. 50). This is well-supported by data in sunitinib-treated patients with RCC where reduction in the levels of Treg cells is correlated with increased IFNγ secreting T cells (52). In this study, ODM-203 favored an increase in the ratio of T cells to Tregs thus leading to an immune stimulatory environment enabling a successful immune response to tumor (Fig. 5A). Axitinib-regulated NK-cell-activating ligand expression in RCC cells, thus enhancing NK-cell recognition and activation (54), which was also evinced by increased IFNγ levels in ODM-203 treated group by NK cells (Fig. 5B).

Potent antitumor activity as a result of a combination of direct antiproliferative activity in FGFR-altered cancer cell lines, anti-angiogenesis activity and antitumor immunity reported here supports the continued clinical development of ODM-203 for improved outcomes in patients with angiogenic tumors harboring genomic alterations in the FGFR signaling pathway.

Disclosure of Potential Conflicts of Interest

T.H. Holmström is Head of Biologics at Orion Corporation Orion Pharma. T. Linnanen has ownership interest (including stock, patents, etc.) in one of the inventions in ODM-203 patent, all rights given to Orion Pharma. R. Oksala has ownership interest (including stock, patents, etc.). No potential conflicts of interest were disclosed by the other authors.

Authors' Contributions

Conception and design: T.H. Holmström, A.-M. Moilanen, T. Ikonen, T. Linnanen, G. Wohlfahrt, S. Samajdar, S. Rajagopalan, N. Gowda, S. Mukherjee, R.K. Ujjinamatada, N. Srinivas, M. Ramachandra, P.J. Kallio

Development of methodology: T.H. Holmström, A.-M. Moilanen, M.L. Björkman, R. Oksala, S. Samajdar, S. Rajagopalan, K. Narayan, R.K. Ramachandra, J. Mani, N. Gowda, S. Dhodheri, N. Srinivas, M. Ramachandra

Acquisition of data (provided animals, acquired and managed patients, provided facilities, etc.): T.H. Holmström, A.-M. Moilanen, T. Ikonen, R. Oksala, T. Korjamo, R.K. Ramachandra, J. Mani, R. Nair, T. Anthony, S. Dhodheri, P.J. Kallio

Analysis and interpretation of data (e.g., statistical analysis, biostatistics, computational analysis): T.H. Holmström, A.-M. Moilanen, T. Ikonen, M.L. Björkman, T. Linnanen, G. Wohlfahrt, S. Karlsson, R. Oksala, T. Korjamo, S. Rajagopalan, S. Rajagopalan, K. Narayan, R.K. Ramachandra, J. Mani, R. Nair, N. Gowda, T. Anthony, S. Dhodheri, S. Mukherjee, M. Ramachandra, P.J. Kallio
Writing, review, and/or revision of the manuscript: T.H. Holmström, A.-M. Moilanen, T. Ikonen, M.L. Björkman, G. Wohlfahrt, R. Oksala, T. Korjamo, S. Rajagopalan, S. Rajagopalan, K. Narayan, R.K. Ramachandra, J. Mani, R. Nair, N. Gowda, S. Dhodheri, M. Ramachandra, P.J. Kallio
Administrative, technical, or material support (i.e., reporting or organizing data, constructing databases): T.H. Holmström, M.L. Björkman, S. Rajagopalan, S. Rajagopalan, K. Narayan, T. Anthony
Study supervision: T.H. Holmström, A.-M. Moilanen, T. Linnanen, S. Samajdar, S. Rajagopalan, S. Rajagopalan, S. Chelur, K. Narayan, N. Gowda, S. Dhodheri, N. Srinivas, M. Ramachandra, P.J. Kallio

Other (Lead Medicinal chemist at Orion in ODM-203 project: T. Linnanen
Other (synthesis of molecules): S. Samajdar

Acknowledgments

This work was supported by Orion Corporation Orion Pharma.

The costs of publication of this article were defrayed in part by the payment of page charges. This article must therefore be hereby marked *advertisement* in accordance with 18 U.S.C. Section 1734 solely to indicate this fact.

Received March 9, 2018; revised August 20, 2018; accepted October 4, 2018; published first October 9, 2018.

References

1. Beenken A, Mohammadi M. The FGF family: biology, pathophysiology and therapy. Nat Rev Drug Discov 2009;8:235–53.
2. Turner N, Grose R. Fibroblast growth factor signalling: from development to cancer. Nat Rev Cancer 2010;10:116–29.
3. Hadari YR, Gotoh N, Kouhara H, Lax I, Schlessinger J. Critical role for the docking-protein FRS2 alpha in FGF receptor-mediated signal transduction pathways. Proc Natl Acad Sci U S A 2001;98:8578–83.
4. Ong SH, Guy GR, Hadari YR, Laks S, Gotoh N, Schlessinger J, et al. FRS2 proteins recruit intracellular signaling pathways by binding to diverse targets on fibroblast growth factor and nerve growth factor receptors. Mol Cell Biol 2000;20:979–89.
5. Kouhara H, Hadari YR, Spivak-Kroizman T, Schilling J, Bar-Sagi D, Lax I, et al. A lipid-anchored Grb2-binding protein that links FGF-receptor activation to the Ras/MAPK signaling pathway. Cell 1997; 89:693–702.
6. Javerzat S, Auguste P, Bikfalvi A. The role of fibroblast growth factors in vascular development. Trends Mol Med 2002;8:483–9.
7. Lieu C, Heymach J, Overman M, Tran H, Kopetz S. Beyond VEGF: inhibition of the fibroblast growth factor pathway and antiangiogenesis. Clin Cancer Res 2011;17:6130–9.
8. Touat M, Ileana E, Postel-Vinay S, Andre F, Soria JC. Targeting FGFR signaling in cancer. Clin Cancer Res 2015;21:2684–94.
9. Giavazzi R, Sennino B, Coltrini D, Garofalo A, Dossi R, Ronca R, et al. Distinct role of fibroblast growth factor-2 and vascular endothelial growth factor on tumor growth and angiogenesis. Am J Pathol 2003; 162:1913–26.
10. Batchelor TT, Sorensen AG, di Tomaso E, Zhang WT, Duda DG, Cohen KS, et al. AZD2171, a pan-VEGF receptor tyrosine kinase inhibitor, normalizes tumor vasculature and alleviates edema in glioblastoma patients. Cancer Cell 2007;11:83–95.
11. Casanovas O, Hicklin DJ, Bergers G, Hanahan D. Drug resistance by evasion of antiangiogenic targeting of VEGF signaling in late-stage pancreatic islet tumors. Cancer Cell 2005;8:299–309.
12. Saylor PJ, Escudier B, Michaelson MD. Importance of fibroblast growth factor receptor in neovascularization and tumor escape from antiangiogenic therapy. Clin Genitourin Cancer 2012;10:77–83.
13. Bange J, Prechtl D, Cheburkin Y, Specht K, Harbeck N, Schmitt M, et al. Cancer progression and tumor cell motility are associated with the FGFR4 Arg(388) allele. Cancer Res 2002;62:840–7.
14. Carrillo de Santa Pau E, Arias FC, Caso Pelaez E, Munoz Molina GM, Sanchez Hernandez I, Muguruza Trueba I, et al. Prognostic significance of the expression of vascular endothelial growth factors A, B, C, and D and their receptors R1, R2, and R3 in patients with nonsmall cell lung cancer. Cancer 2009;115:1701–12.
15. Cihoric N, Savic S, Schneider S, Ackermann I, Bichsel-Naef M, Schmid RA, et al. Prognostic role of FGFR1 amplification in early-stage non-small cell lung cancer. Br J Cancer 2014;110:2914–22.
16. Decaussin M, Sartelet H, Robert C, Moro D, Claraz C, Brambilla C, et al. Expression of vascular endothelial growth factor (VEGF) and its two receptors (VEGF-R1-Flt1 and VEGF-R2-Flk1/KDR) in non-small cell lung carcinomas (NSCLCs): correlation with angiogenesis and survival. J Pathol 1999;188:369–77.
17. Elbauomy Elsheikh S, Green AR, Lambros MB, Turner NC, Grainge MJ, Powe D, et al. FGFR1 amplification in breast carcinomas: a chromogenic in situ hybridisation analysis. Breast Cancer Res 2007;9:R23.
18. Ghosh S, Sullivan CA, Zerkowski MP, Molinaro AM, Rimm DL, Camp RL, et al. High levels of vascular endothelial growth factor and its receptors (VEGFR-1, VEGFR-2, neuropilin-1) are associated with worse outcome in breast cancer. Hum Pathol 2008;39:1835–43.
19. Juttner S, Wissmann C, Jons T, Vieth M, Hertel J, Gretschel S, et al. Vascular endothelial growth factor-D and its receptor VEGFR-3: two novel independent prognostic markers in gastric adenocarcinoma. J Clin Oncol 2006;24:228–40.
20. Murase H, Inokuchi M, Takagi Y, Kato K, Kojima K, Sugihara K. Prognostic significance of the co-overexpression of fibroblast growth factor receptors 1, 2 and 4 in gastric cancer. Mol Clin Oncol 2014;2:509–17.
21. Mylona E, Alexandrou P, Mpakali A, Giannopoulou I, Liapis G, Markaki S, et al. Clinicopathological and prognostic significance of vascular endothelial growth factors (VEGF)-C and -D and VEGF receptor 3 in invasive breast carcinoma. Eur J Surg Oncol 2007;33:294–300.
22. Ozdemir F, Akdogan R, Aydin F, Reis A, Kavgaci H, Gul S, et al. The effects of VEGF and VEGFR-2 on survival in patients with gastric cancer. J Exp Clin Cancer Res 2006;25:83–8.
23. Seo AN, Jin Y, Lee HJ, Sun PL, Kim H, Jheon S, et al. FGFR1 amplification is associated with poor prognosis and smoking in non-small-cell lung cancer. Virchows Arch 2014;465:547–58.
24. Seto T, Higashiyama M, Funai H, Imamura F, Uematsu K, Seki N, et al. Prognostic value of expression of vascular endothelial growth factor and its flt-1 and KDR receptors in stage I non-small-cell lung cancer. Lung Cancer 2006;53:91–6.
25. Chouaib S, Messai Y, Couve S, Escudier B, Hasmim M, Noman MZ. Hypoxia promotes tumor growth in linking angiogenesis to immune escape. Front Immunol 2012;3:21–30.
26. Huang Y, Goel S, Duda DG, Fukumura D, Jain RK. Vascular normalization as an emerging strategy to enhance cancer immunotherapy. Cancer Res 2013;73:2943–8.
27. Dirkx AE, oude Egbrink MG, Castermans K, van der Schaft DW, Thijssen VL, Dings RP, et al. Anti-angiogenesis therapy can overcome endothelial cell anergy and promote leukocyte-endothelium interactions and infiltration in tumors. FASEB J 2006;20:621–30.
28. Huang Y, Lei L, Liu D, Jovin I, Russell R, Johnson RS, et al. Normal glucose uptake in the brain and heart requires an endothelial cell-specific HIF-1alpha-dependent function. Proc Natl Acad Sci U S A 2012;109:17478–83.
29. Shrimali RK, Yu Z, Theoret MR, Chinnasamy D, Restifo NP, Rosenberg SA. Antiangiogenic agents can increase lymphocyte infiltration into tumor and enhance the effectiveness of adoptive immunotherapy of cancer. Cancer Res 2010;70:6171–80.
30. Gavine PR, Mooney L, Kilgour E, Thomas AP, Al-Kadhimi K, Beck S, et al. AZD4547: an orally bioavailable, potent, and selective inhibitor of the fibroblast growth factor receptor tyrosine kinase family. Cancer Res 2012;72:2045–56.
31. Guagnano V, Kauffmann A, Wohrle S, Stamm C, Ito M, Barys L, et al. FGFR genetic alterations predict for sensitivity to NVP-BGJ398, a selective pan-FGFR inhibitor. Cancer Discov 2012;2:1118–33.

32. Zhao G, Li WY, Chen D, Henry JR, Li HY, Chen Z, et al. A novel, selective inhibitor of fibroblast growth factor receptors that shows a potent broad spectrum of antitumor activity in several tumor xenograft models. Mol Cancer Ther 2011;10:2200–10.
33. Bello E, Colella G, Scarlato V, Oliva P, Berndt A, Valbusa G, et al. E-3810 is a potent dual inhibitor of VEGFR and FGFR that exerts antitumor activity in multiple preclinical models. Cancer Res 2011;71:1396–405.
34. Hilberg F, Roth GJ, Krssak M, Kautschitsch S, Sommergruber W, Tontsch-Grunt U, et al. BIBF 1120: triple angiokinase inhibitor with sustained receptor blockade and good antitumor efficacy. Cancer Res 2008;68:4774–82.
35. Huynh H, Ngo VC, Fargnoli J, Ayers M, Soo KC, Koong HN, et al. Brivanib alaninate, a dual inhibitor of vascular endothelial growth factor receptor and fibroblast growth factor receptor tyrosine kinases, induces growth inhibition in mouse models of human hepatocellular carcinoma. Clin Cancer Res 2008;14:6146–53.
36. Sarker D, Molife R, Evans TR, Hardie M, Marriott C, Butzberger-Zimmerli P, et al. A phase I pharmacokinetic and pharmacodynamic study of TKI258, an oral, multitargeted receptor tyrosine kinase inhibitor in patients with advanced solid tumors. Clin Cancer Res 2008; 14:2075–81.
37. Ahnert JR, Garratt C, Laapas K, Leskinen H, Bjorklund H, Ruck A, et al. Dose escalation study of ODM-203, a selective dual FGFR/VEGFR inhibitor, in patients with advanced solid tumours. J Clin Oncol 2016;34:2576.
38. Weiss J, Sos ML, Seidel D, Peifer M, Zander T, Heuckmann JM, et al. Frequent and focal FGFR1 amplification associates with therapeutically tractable FGFR1 dependency in squamous cell lung cancer. Sci Transl Med 2010;2:62ra93.
39. Kunii K, Davis L, Gorenstein J, Hatch H, Yashiro M, Di Bacco A, et al. FGFR2-amplified gastric cancer cell lines require FGFR2 and Erbb3 signaling for growth and survival. Cancer Res 2008;68:2340–8.
40. Williams SV, Hurst CD, Knowles MA. Oncogenic FGFR3 gene fusions in bladder cancer. Hum Mol Genet 2013;22:795–803.
41. Carmeliet P, Jain RK. Molecular mechanisms and clinical applications of angiogenesis. Nature 2011;473:298–307.
42. Ellis L, Hammers H, Pili R. Targeting tumor angiogenesis with histone deacetylase inhibitors. Cancer Lett 2009;280:145–53.
43. Folkman J. Angiogenesis: an organizing principle for drug discovery? Nat Rev Drug Discov 2007;6:273–86.
44. Bishop ET, Bell GT, Bloor S, Broom IJ, Hendry NF, Wheatley DN. An in vitro model of angiogenesis: basic features. Angiogenesis 1999;3: 335–44.
45. Wolfe A, O'Clair B, Groppi VE, McEwen DP. Pharmacologic characterization of a kinetic in vitro human co-culture angiogenesis model using clinically relevant compounds. J Biomol Screen 2013;18:1234–45.
46. Acevedo VD, Ittmann M, Spencer DM. Paths of FGFR-driven tumorigenesis. Cell Cycle 2009;8:580–8.
47. Chang YS, Adnane J, Trail PA, Levy J, Henderson A, Xue D, et al. Sorafenib (BAY 43–9006) inhibits tumor growth and vascularization and induces tumor apoptosis and hypoxia in RCC xenograft models. Cancer Chemother Pharmacol 2007;59:561–74.
48. Manning EA, Ullman JG, Leatherman JM, Asquith JM, Hansen TR, Armstrong TD, et al. A vascular endothelial growth factor receptor-2 inhibitor enhances antitumor immunity through an immune-based mechanism. Clin Cancer Res 2007;13:3951–9.
49. Liu L, Ye TH, Han YP, Song H, Zhang YK, Xia Y, et al. Reductions in myeloid-derived suppressor cells and lung metastases using AZD4547 treatment of a metastatic murine breast tumor model. Cell Physiol Biochem 2014;33: 633–45.
50. Kwilas AR, Ardiani A, Donahue RN, Aftab DT, Hodge JW. Dual effects of a targeted small-molecule inhibitor (cabozantinib) on immune-mediated killing of tumor cells and immune tumor microenvironment permissiveness when combined with a cancer vaccine. J Transl Med 2014;12:294–308.
51. Kwilas AR, Donahue RN, Tsang KY, Hodge JW. Immune consequences of tyrosine kinase inhibitors that synergize with cancer immunotherapy. Cancer Cell Microenviron 2015;2:677–87.
52. Finke JH, Rini B, Ireland J, Rayman P, Richmond A, Golshayan A, et al. Sunitinib reverses type-1 immune suppression and decreases T-regulatory cells in renal cell carcinoma patients. Clin Cancer Res 2008;14:6674–82.
53. Pal SK, Hossain DM, Zhang Q, Frankel PH, Jones JO, Carmichael C, et al. Pazopanib as third line therapy for metastatic renal cell carcinoma: clinical efficacy and temporal analysis of cytokine profile. J Urol 2015;193:1114–21.
54. Morelli MB, Amantini C, Santoni M, Soriani A, Nabissi M, Cardinali C, et al. Axitinib induces DNA damage response leading to senescence, mitotic catastrophe, and increased NK cell recognition in human renal carcinoma cells. Oncotarget 2015;6:36245–59.